What are the Implications of Nonequilibrium in the $O+OH$ and $O+HO_2$ Reactions?

A. J. C. Varandas*[a]

*Vibrationally excited O_2, OH, and HO_2 species have been suggested (J. Phys. Chem. A **2004**, 108, 758) to provide clues for explaining the "ozone deficit problem" and "HO_x dilemma" in the middle atmosphere under conditions of local thermodynamic disequilibrium (LTD), but the question arises of how much LTD will affect the title ozone sink reactions. Besides providing novel kinetic results, it is shown that LTD tends to disfavor ozone depletion relative to traditional atmospheric modeling under Boltzmann equilibration, which is partly due to competition between the various reactive channels. The calculations also suggest that the title LTD processes can be important sources of highly vibrationally excited O_2 in the middle atmosphere. Moreover, LTD is shown to offer an explanation for the fact that some down revision of the $O+HO_2$ rate constant, or the ratio of the $O+HO_2$ to $O+OH$ rate constants, is required to improve agreement between the predictions of traditional modeling and observation. This, in turn, provides significant evidence supporting LTD at such altitudes.*

1. Introduction

Atmospheric ozone has the potential to change the biological makeup and possibly the climate of the planet, and thus it is among the chemical species whose impact on earth has been the most extensively studied. Traditionally, its production is believed to occur via photodissociation of atmospheric O_2 by solar ultraviolet radiation,[1] followed by $O+O_2$ three-body recombination. Conventional photochemical modeling is reasonably accurate in predicting altitude-dependent profiles in the lower stratosphere, but aircraft observations suggest that it significantly underpredicts the O_3 abundance at higher altitudes. This finding led to the proposition of alternative ozone sources.[2–6]

The first attempt to explain the O_3 deficit in the stratosphere is the Chapman-like (all-oxygen) mechanism proposed by Wodtke and co-workers:[4]

$$O_3 + h\nu \rightarrow O_2(v) + O \quad (1)$$

$$O_2(v) + O_2 \rightarrow O_3 + O \quad (2)$$

$$2 \times \{O + O_2 + M \rightarrow O_3 + M\} \quad (3)$$

$$\text{Net}: \; 3O_2 + h\nu \rightarrow 2O_3 \quad (4)$$

where v (for a larger polyatomic, we denote the complete set of vibrational quantum numbers by $\boldsymbol{v}$) identifies a species in a high vibrationally excited state. Unfortunately, direct evidence that O_3 is formed in reaction (2) is lacking,[7,8] with the caveat extending to theoretical studies.[9–17] However, O_3 may be formed when both O_2 molecules are vibrationally excited, although the efficiency depends on the chance of such a bimolecular process to occur.[5,18] Note that past and current theoretical studies are based on the premise of adiabaticity, and hence the relevance of nonadiabatic effects in explaining the results of Wodtke et al. is open to debate.[17,19]

Despite steady efforts in observation and theory, giving the impression in the 1990s[20–24] that the "ozone deficit problem" had been clarified, difficulties persisted[22] in the middle atmosphere (upper stratosphere and mesosphere), while the so-called "HO_x dilemma" also emerged.[25] This is related to odd-hydrogen (OH and HO_2), which is produced by photolysis above 60 km and by:

$$H_2O + O(^1D) \rightarrow OH + OH \quad (5)$$

below that altitude. Briefly, Summers et al.[26] reported measurements of OH between 50 and 80 km that were 25–30% lower than those expected by standard photochemical theory, while balloon-borne simultaneous measurements of OH and HO_2 by Sandor and Clancy[27] indicated $[HO_2]$ to be 25–30% higher than expected. In turn, Jucks et al.[28] found that measured [OH] agrees reasonably well with, and measured $[HO_2]$ is significantly higher than, values calculated using standard kinetic parameters at 40–50 km. The conflict between theory and observation culminated with the finding by Conway et al.[25] that mesospheric OH densities are 25–35% lower than those predicted by standard photochemical theory, although the observed OH density increases rapidly below 50 km to become 20% or so larger than that calculated at about 43 km. This led to a dilemma since the standard procedure in atmospheric modeling consists of achieving agreement with observation by rate-constant scaling, in this case for the reactions:

$$O + OH \rightarrow O_2 + H \quad (6)$$

$$O + HO_2 \rightarrow O_2 + OH \quad (7)$$

[a] *Prof. A. J. C. Varandas*
Departamento de Química, Universidade de Coimbra
3004-535 Coimbra (Portugal)
Fax: (+351) 239-835867
E-mail: varandas@qtvs1.qui.uc.pt

Supporting information for this article is available on the WWW under http://www.chemphyschem.org or from the author.

 DOI: 10.1002/cphc.200400335

which drive OH/HO_2 partitioning in the middle atmosphere to be controlled by:

$$\frac{[OH]}{[HO_2]} = \frac{k_7}{k_6} \quad (8)$$

Note that the atomic hydrogen produced in reaction (6) reacts with O_2 in the presence of a third body[29,30] to yield HO_2[31] or, eventually, with O_3 to form OH(v) and O_2.[32] However, it is unlikely that a reduction[33] in k_7 or the ratio k_7/k_6 would decrease [OH] in the mesosphere and, simultaneously, increase [OH] at lower altitudes. Despite some improvement in explaining the [OH] and [HO_2] profiles, such a procedure cannot really help to fully unravel the "O_3 deficit problem" and the "HO_x dilemma". Recently,[6] we proposed a theory that seems capable of rationalizing the imbalance in the [OH] and [HO_2] profiles while offering an additional source of O_3 at altitudes where the model of Wodtke et al.[22] is ineffective.

The simplest of such schemes[6] that may enhance O_3 production is:

$$3[H + O_3 \rightarrow OH(v') + O_2] \quad (9)$$

$$OH + O_3 \rightarrow H + O_2(v) + O_2 \quad (10)$$

$$4[O_3 + h\nu \rightarrow O_2(v'') + O] \quad (11)$$

$$OH(v') + O_2(v'') \rightarrow O_3 + H \quad (12)$$

$$OH(v') + O_2(v'') \rightarrow O_2 + O + H \quad (13)$$

$$OH(v') + O_2(v'') \rightarrow OH + 2O \quad (14)$$

$$O_2(v) + O_2(v'') \rightarrow O_3 + O \quad (15)$$

$$8[O + O_2 + M \rightarrow O_3 + M] \quad (16)$$

$$\text{Net}: \ 3O_2 + 4h\nu \rightarrow 2O_3 \quad (17)$$

In turn, the following mechanism has been suggested[6,34] to explain the general pattern of the observed [OH] and [HO_2] vertical profiles:

$$5[H + O_3 \rightarrow OH(v') + O_2] \quad (18)$$

$$3[OH(v') + O_3 \rightarrow HO_2(\boldsymbol{v}) + O_2] \quad (19)$$

$$OH(v') + O_3 \rightarrow 2O_2 + H \quad (20)$$

$$OH(v') + M \rightarrow OH + M \quad (21)$$

$$OH + O_3 \rightarrow HO_2 + O_2 \quad (22)$$

$$HO_2(\boldsymbol{v}) + O_3 \rightarrow OH + 2O_2 \quad (23)$$

$$HO_2(\boldsymbol{v}) + M \rightarrow HO_2 + M \quad (24)$$

$$HO_2 + O_3 \rightarrow OH + 2O_2 \quad (25)$$

$$HO_2(\boldsymbol{v}) \rightarrow H + O_2 \quad (26)$$

$$\text{Net}: \ 3H + 12O_3 \rightarrow HO_2 + 16O_2 + 2OH \quad (27)$$

where reactions (20) and (26) are nonconventional sources of atomic hydrogen. Note that most of the above elementary processes have been the subject of detailed dynamics calculations in our group,[5,18,35–39] while the resulting kinetic equations have in both cases been solved by using[6] the stationary-state assumption. A key premise is that vibrationally excited O_2, OH, and HO_2 species should be abundant enough in the middle atmosphere. In fact, diatomic molecules such as O_2 near the dissociation limit are known to require 10^5–10^6 collisions to deexcite in the presence of inert species, such as Ar atoms,[40] while reactions involving highly vibrationally excited diatomic molecules have been found[5,37,38] to have rate constants for reaction much larger than those of the corresponding relaxation processes. Moreover, both the photolysis of O_3 and the reaction $H + O_3 \rightarrow OH + O_2$ [the major sources of $O_2(v)$ and OH(v) at such altitudes, respectively] occur significantly faster than vibrational relaxation. Thus, in addition to other sources, such as the reactions described herein, these processes can provide a continuous flux of such vibrationally hot species, and hence keep their abundances nearly stationary. Unfortunately, although work is in progress in our group, no data exist at present on the vibrational relaxation rate constant of HO_2. On the other hand, intuition suggests that vibrationally excited species should be more the rule than the exception in the middle atmosphere. Suffice it to recall that the thermosphere (this lies just above the mesosphere) is known to be largely composed of atoms and ionized species, such as N, O, N_2^+, O_2^+, and NO^+ (also partly present in the mesosphere itself), and hence vibrationally hot species should be abundant at such altitudes. This fact supports the hypothesis of local thermodynamic disequilibrium or LTD (commonly referred to as nonlocal thermodynamic equilibrium or NLTE), since the thermosphere is known to deviate significantly from thermal equilibration. Of course, the LTD assumption can only be validated by ultimately comparing its predictions with observation. For example, it is crucial to know whether vibrational excitation enhances odd-oxygen (ozone) destruction via reactions (6) and (7). If the title reactions were equally affected, the ratio in Equation (8) would not change. It is on such an issue that we focus here by running trajectories under LTD. A final remark to note is that accurate reactive quantum dynamics is currently unaffordable to treat the $O + HO_2$ reaction, especially under the nonequilibrium conditions considered here, due to the large number of open channels. Moreover, a comparison of exact classical with approximate quantum calculations for the $H + O_3$[41] and $O + HO_2$[42] reactions using the same potential energy surface has shown that quantum effects should not play a prominent role, thus supporting our use of the (quasi-) classical trajectory (QCT) approach.

The paper is organized as follows: Section 2 summarizes the methodology employed in the trajectory calculations, while the applications to the O + OH and $O + HO_2$ reactions are re-

ported in Section 3. The possible implications of the results in atmospheric modeling are discussed in Section 4 and the major conclusions are presented in Section 5.

2. Method

All calculations employ the QCT method as implemented in the MERCURY/VENUS96[43] codes, and cover temperatures of interest in the middle atmosphere (they vary from $T \approx 270$ K in the stratopause at ≈ 15 km down to ≈ 190 K in the mesopause at ≈ 85 km). For completeness, a few extra temperatures were considered outside that range, although the chosen micropopulations can hardly be justified for such regimes. To study the O+OH reaction, we used the popular HO_2 DMBE IV[44] potential energy surface (DMBE = double many-body expansion) while, for O+HO_2, both the HO_3 DMBE I[45] and DMBE II[46] surfaces were employed. Their energetics is illustrated in Figure 1.

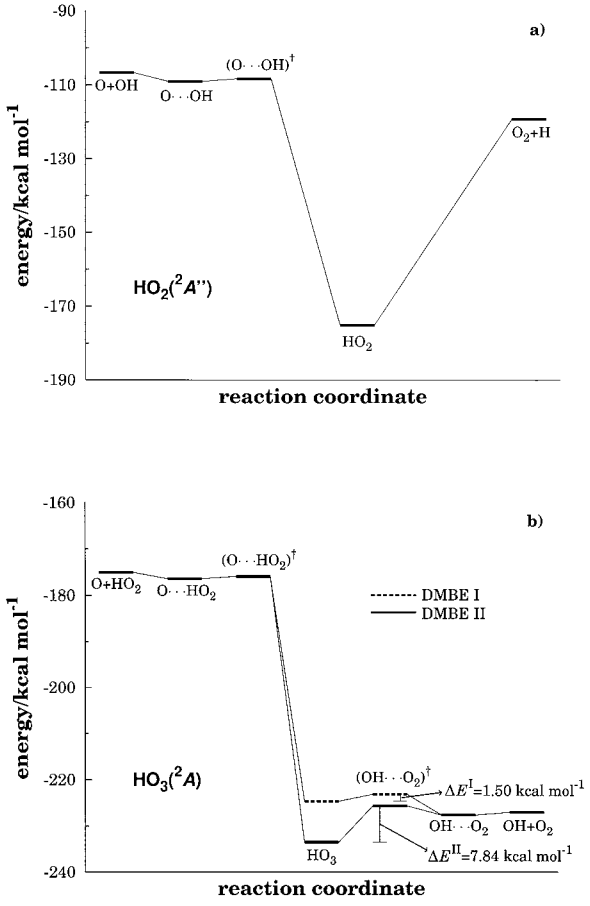

Figure 1. *Energetics of the title reactions based on the DMBE potential energy surfaces used in this work. a) O+OH; b) O+HO_2.*

The initial conditions were chosen as follows. The collision energy (E_{tr}) is selected from a Maxwell–Boltzmann distribution by using the cumulative function:[47]

$$G(E_{tr}) = \left(\frac{1}{k_B T}\right)^2 \int_0^{E_{tr}} E_{tr}' \exp(-E_{tr}'/k_B T)\,dE_{tr}' \qquad (28)$$

where E_{tr} is chosen randomly for each trajectory by solving the equation $G(E_{tr})-\xi_1=0$; ξ_k ($k=1$–3) denotes hereafter a random number, and k_B is the Boltzmann constant. In turn, the vibrational and rotational quantum numbers (v' and j') of the reactant OH were sampled by using a cumulative distribution function of the type:

$$C(E) = \sum_{n=0}^{v'j'} P(n) \qquad (29)$$

where $P(n)$ may be a pure vibrational distribution or a rotational distribution for a given v' state. The simulation of a specific ($v'j'$) state therefore involves two steps. First, the summation in Equation (29) is allowed to run from the lowest vibrational level up to the v' value that satisfies $C(E_v')-\xi_2=0$. Using this value of v', the summation in Equation (29) is carried up to the rotational state j' that satisfies[48] $C(E_{j';v})-\xi_3=0$. For the vibrational micropopulations of OH, $P(v')$ was chosen to be the "steady-state" distribution[49] reported elsewhere,[39] which is compared with the corresponding "nascent" distribution[50] from the reaction H+O_3→OH+O_2 in Figure 2. Clearly, the similarity of these distributions questions the traditional assumption of thermal equilibration in atmospheric modeling. In turn, the rotational distribution of OH is the "steady-state" distribution[39] obtained by molecular simulation from Cosby's[51] effective nascent rotational micropopulation.[52]

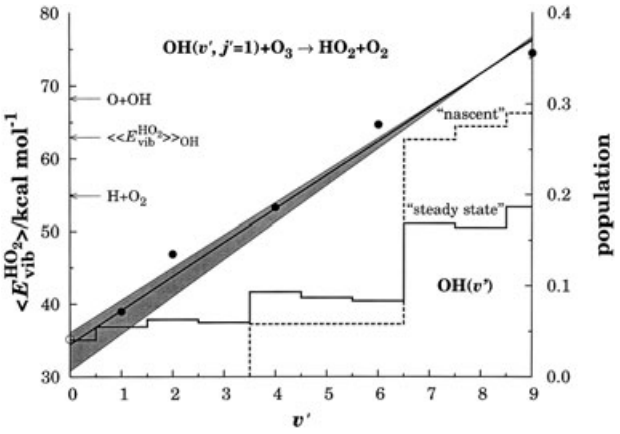

Figure 2. *Average vibrational energy of HO_2 in the reaction OH(v)+O_3→ HO_2+O_2. The dots (●) indicate the calculated[54,55] values for $E_{tr}=1.0$ kcal mol^{-1} while the solid line (——) denotes their least-squares fit $\langle E_{int}^{HO_2}\rangle$/kcal mol^{-1} $=34.5+4.6v'$ (this nearly coincides with the curve for T = 354.3 K). The shaded area is delimited at the top (bottom) by the curve for T = 110 K (450 K). Also shown is the H+O_2 dissociation energy, and the mean vibrational ($\langle\langle E_{vib}^{HO_2}\rangle\rangle_{OH}$) energy of HO_2 averaged over v'. The open circle (○) indicates the value of $\langle E_{vib}^{HO_2}\rangle$ calculated[32] for v' = 0 at $E_{tr}=8.0$ kcal mol^{-1}. The y axis on the right-hand side refers to the nascent and "steady-state"[39] distributions of OH(v').*

No experimental information is available on the micropopulations of HO_2, whose main source[53] in the middle atmosphere is the reaction OH(v')+O_3→HO_2(E_{vib})+O_2; where indicated, the dependence on E_{vib} implies that vibrational quantum numbers are not explicitly attributed. Thus, we employ the results predicted from our own calculations.[54,55] The idea is to relate the

vibrational distribution of $HO_2(\boldsymbol{v})$ to that of $OH(v')$, since the average vibrational excitation of the nascent HO_2 radicals has been calculated as a function of v'. Unfortunately, the results are available for specific translational energies rather than temperatures, but these may be approximated from the former by $\langle E_{tr}\rangle = \frac{3}{2}k_B T$. Since, except in a few cases, the calculations[54,55] were carried out only down to a translational energy of (335.5 K), we fitted the results to the form:

$$\langle E_{vib}^{HO_2}\rangle(v';E_{tr}) = A(E_{tr}) + B(E_{tr})v' \quad (30)$$

and used the two lowest-studied translational energies ($E_{vib}=1$ and 2 kcal mol^{-1} for $v'=1$–9) to extrapolate the distributions to the temperatures here considered. To improve the behavior near the threshold, a weight of two was assigned to the points with $v'=1$ in the least-squares fit of Equation (30); for an equally weighted fit, see ref. [6]. One gets $A(E_{tr})$/kcal mol^{-1} = 29.8059 + 4.6706E_{tr} and $B(E_{tr})$/kcal mol^{-1} = 5.2234 − 0.5739E_{tr} which, say for $T=210$ K, predict the nascent vibrational energy distribution of HO_2 to be given by $\langle E_{vib}^{HO_2}\rangle$/kcal mol^{-1} = 32.7296 + 4.8642v'. It is this form that is employed for $T=210$ K, with corresponding functions being used for other temperatures.[56] Note that the above scheme leads to $\langle E_{vib}^{HO_2}\rangle = 34.7$ kcal mol^{-1} for $v'=0$ at a temperature (354.3 K) corresponding to the reaction threshold,[32] which is close to the value of $\langle E_{vib}^{HO_2}\rangle$ = 35.2 kcal mol^{-1} calculated[32] for $E_{tr}=8$ kcal mol^{-1}. Note further that the vibrational excitation of HO_2 (sometimes above the dissociation threshold and then indicated by HO_2^*) increases with the vibrational state of OH. This should not be surprising since the classical exothermicity of the $OH+O_3$ reaction is $\Delta H_{class} = -51.94$ kcal mol^{-1}, and the energy release in the products' HO_2 vibration is typically 50–60%.[54,55] We emphasize that a rigorous way of obtaining the nascent vibrational energy distribution of HO_2 would be to perform calculations of the $OH+O_3$ reaction at each temperature using the "steady-state" micropopulations, a computational burden that is deemed unjustified here. Naturally, the use of a "steady-state" vibrational energy distribution for $HO_2(\boldsymbol{v})$ might bring additional realism, but this too is unavailable at present.

We now address the fact that the average energy channeled into vibration of HO_2 is much larger than the zero-point energy (ZPE = 8.5 kcal mol^{-1}). Although HO_2^* could be taken a priori as dissociative to give $H+O_2$ or $O+OH$, this has not been done as the true outcome may depend on whether there is a collision before the unimolecular dissociation process occurs. Thus, we chose to initiate the trajectories with the HO_2 vibrational excitations given by Equation (30). Once the vibrational energy is defined, the standard fixed normal-mode sampling procedure[43] is used to distribute it by the three vibrational normal modes of HO_2.[57] Such a democratic partition of the vibrational energy should be plausible since, for high vibrational excitations, the nuclear motion tends to be classically chaotic.[58,59] To complete the specification of the initial internal energy of HO_2, the rotational energy about each principal axis of inertia of the triatomic species has been set equal to $k_B T/2$.

Unavoidably, one has the problem of ZPE leakage when running classical trajectories. Both "active" and "nonactive" fixes have been proposed,[55,60–66] but none is free of some ambiguity, with the only exact solution being via quantum mechanics. Here we are dealing with high vibrational excitations, so the problem may be ignored without significant error, as indeed the results seem to suggest. Another subtle issue refers to the assignment of internal quantum states to the products. This and other technical issues are discussed in the Supporting Information.

3. Results and Discussion

3.1. The O + OH Reaction

The O + OH reaction has been much studied using both quasiclassical[67–73] and approximate quantum[74] dynamics because of its key role in the atmosphere, and the fact that it is the reverse of the most important reaction in combustion. Most such studies employed the DMBE IV[44] potential energy surface for ground-state HO_2, which will also be used herein. The rate constant for quenching of $OH(v')$ in collisions with oxygen atoms plays a critical role in establishing the populations of the various v' states and ultimately describes the OH nightglow in the middle atmosphere;[75] however, no such studies had been reported for $v'\geq 1$ until completion of the present work.

In addition to the inelastic channel:

$$O_a + O_bH(v_i',j_i') \rightarrow O_bH(v_f',j_f') + O_a \quad (31)$$

two reactive channels are open under the initial conditions here considered:

$$O_a + O_bH(v',j') \rightarrow O_aO_b(v'',j'') + H \quad (32)$$

$$O_a + O_bH(v',j') \rightarrow O_aH(v'',j'') + O_b \quad (33)$$

where the indices (a and b) distinguish the oxygen atoms. Reactions (32) and[76] (33) are both affected by vibrationally exciting OH, thus a prediction of this effect on their relative importance is nontrivial. This may have implications for a complete understanding of the ozone budget in the atmosphere, since both reactions must be considered when examining the collisions of an oxygen atom with a hydroxyl radical.

Table 1 summarizes the results of the trajectory calculations carried out for the O + OH reaction. It is seen that the reactive probabilities for the channels leading to O_2+H and H-atom exchange have average values of about 12 and 3%, respectively,[77] and hence the sum of the H-atom exchange and nonreactive probabilities is on average 85%. The final OH radicals produced via channels (31) and (33) are indistinguishable, so we may compare the total vibrational distribution with that of the reactants; the reactant quantum numbers are denoted by (v',j') or (v_i',j_i'), with a double prime being used for the products. Such a comparison for $T=255$ K (the results for other temperatures show similar features) is shown in Figure 3a, while Figure 3b shows the corresponding rotational distribution for all vibrational states of O_aH and O_bH. The striking feature is the similarity of the final and initial vibrational–rotational distributions. Clearly, there is a slight tendency to populate vibrational

Table 1. *A summary of the dynamics calculations[a] for the O_a+O_bH reaction.*

					O_aH+O_b		O_aO_b+H
T [K]	b_{max} [Å]	$N/10^4$	P_{nr} [%]	P_r [%]	$k^{[b]}$ [$cm^3 s^{-1}$]	P_r [%]	$k^{[b]}$ [$cm^3 s^{-1}$]
110	11.7	1	83.2	2.8	10.06 ± 0.60	13.6	49.64 ± 1.25
160	11.7	1	86.1	2.6	9.59 ± 0.59	11.9	43.88 ± 1.19
210	11.2	1	86.3	2.5	9.52 ± 0.56	11.8	39.92 ± 1.09
255	10.8	3	86.0	2.7	8.49 ± 0.29	11.6	36.37 ± 0.58
300	10.5	1	85.6	2.8	8.48 ± 0.50	11.3	33.93 ± 0.95
350	10.3	1	86.5	2.7	7.91 ± 0.47	11.1	32.38 ± 0.92
400	10.0	1	86.2	2.8	7.87 ± 0.46	10.8	30.26 ± 0.87
450	9.0	1	83.2	3.3	7.46 ± 0.44	13.2	30.35 ± 0.78

[a] All calculations were carried out employing an optimum step size for the numerical integration of 8×10^{-15} s, with the trajectories being initiated with the reactants 13 Å apart from each other. [b] All rate constants should be multiplied by 10^{-12}.

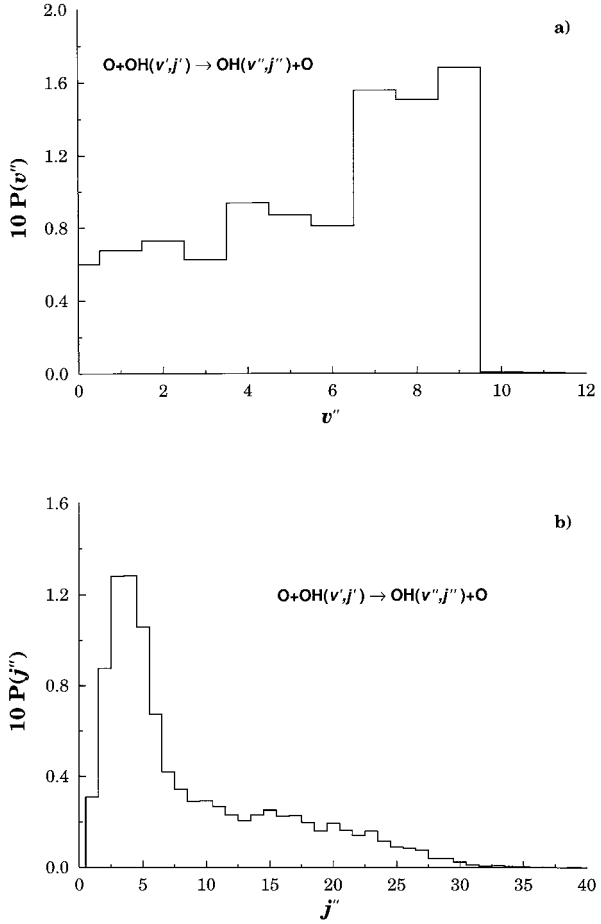

Figure 3. *Final vibrational (a) and rotational (b) distributions of the hydroxyl radicals resulting from both the nonreactive and hydrogen-atom exchange channels in O+OH(v') collisions at T = 255 K.*

states[78] with $v' \leq 3$ at the expense of $v' = 7$–9, while the populations of intermediate levels are left basically unchanged. Parenthetically, we observe that the probability of vibrational de-excitation via the inelastic process (31) follows approximately the exponential-energy-gap law[40] $-\ln[P(\Delta v')] = 3.545 - 0.436\Delta v'$, with the size of the vibrational quantum jump $\Delta v' = v_f' - v_i'$ varying with v_i': vibrational transitions involving one quantum jump for small values of v_i', multiquantum transitions more likely for large v_i'. In turn, Figure 3b shows that the rotational distribution maintains its initial two-temperature character, with a slight increase in the population of high rotational states. This suggests that vibrational-to-rotational energy transfer dominates in nonreactive and H-atom exchange processes. Such a feature is particularly visible for the latter that show a broad maximum at $j' = 15$–20. Besides vibrational de-excitation, one also observes vestige occupations of vibrational states as high as $v' = 10$–13, which were not originally populated. This finding suggests that vibrationally excited species higher than $v' = 9$ may appear in the middle atmosphere, which may corroborate the faint OH($v = 10$) emission line recently detected in the night airglow[79] (see also ref. [39]). Thus, except for those yielding O_2, the O+OH collisions leave the OH radicals with a nearly intact ability for reaction with highly vibrationally excited O_2 to form O_3+H, as discussed elsewhere.[6] Interestingly, H-atom exchange produces OH radicals with vibrational excitations up to the maximum observed values, a pattern that is typical also for other temperatures. Note that ZPE leakage should be most influential for reaction (33), since the one yielding O_2+H is highly exothermic. In fact, for $T = 255$ K, the number of OH radicals that end up with a vibrational energy below the quantum-mechanical ZPE threshold is only 1.5% of all collisions that produce OH radicals. Thus, ZPE leakage should have a minor impact, and hence will be ignored.

Figure 4 shows, for $T = 255$ K, the vibrational distribution of the products $O_2(v'',j'')$ for all v' states of the reactant OH. Despite some fluctuations, it is clearly of non-Boltzmann type, with a nearly flat distribution up to $v'' = 15$ or so, where it starts to decrease and then vanish at $v'' = 26$. Thus, vibrational states almost as high as those formed in the triplet channel of

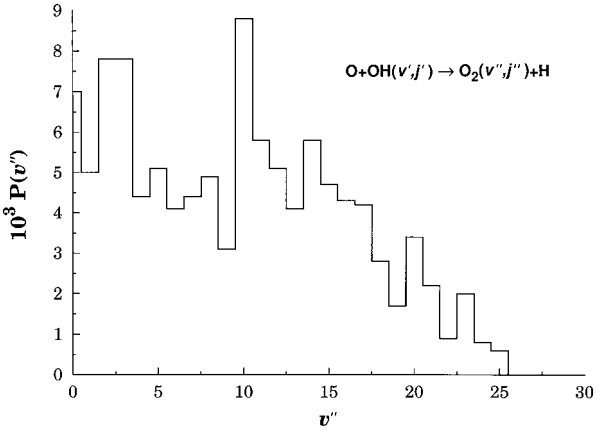

Figure 4. *Vibrational distribution of product $O_2(v'',j'')$ from the LTD O+OH(v',j') reactive collisions at a temperature of 255 K.*

the ozone photodissociation[22] can be observed. Such a process may not have the importance of the latter (even if the triplet channel represents only about 10% of the total ozone photodissociation) in the stratosphere and lower mesosphere, but the reaction (32) should help to maintain the flux of vibrationally hot O_2, especially at higher altitudes where $O(^3P)$ atoms and vibrationally hot OH radicals are abundant. The process may then contribute to ozone formation via collisions of the formed $O_2(v)$ with other highly vibrationally excited O_2 and OH species.[6] To our knowledge, such a source of $O_2(v)$ has not been recognized previously. As for the rotational levels, one observes states as high as $j'' \approx 200$. Moreover, the rotational distribution for all v'' states is well described by a temperature of 15076 K, which may partly be attributed to randomization[58,59] of the reaction exothermicity before the OH breaks off.

Given the unavailability of vibrationally specific thermal rate constants for the quenching of $OH(v')$ in collisions with atomic oxygen, it would appear interesting to report on them at this stage. However, the error bars vary with the weight of the initial vibrational quantum number which, for $v'=0$, is a factor of five smaller than that for $v'=9$. This would lead to undesirable fluctuations in the vibrationally specific rate constants caused by the statistics, therefore we leave a more detailed analysis of such an issue to be presented elsewhere.[80] We emphasize that a few thousand trajectories suffice to get total rate constants converged within the error bars of the recommended[81] values, and it is the result of more conservative estimates that we report here. The rate constants are shown in Figure 5 as a function of temperature, together with a fit to:

$$k(T) = f_e(T)\left[\frac{2^{(3n-4)/2n}n\pi^{1/2}}{(n-2)^{(n-2)/n}\mu^{1/2}}\Gamma\left(\frac{2n-2}{n}\right)C_n^{2/n}(k_BT)^{(n-4)/2n}\right] + f_e(T)\left[\pi\eta^2\left(\frac{8k_BT}{\pi\mu}\right)^{1/2}\right] \quad (34)$$

where $f_e(T) = 2/\{[5+3\exp(-228/T)+\exp(-326/T)][2+2\exp(-205/T)]\}$ is the electronic degeneracy factor, and η is the sum of the radii of the two interacting species taken as rigid spheres; all other symbols have their usual meaning. The effective long-range potential ($V \propto -C_n r^n$) that leads to the above capture[82] plus rigid-spheres-type model is unknown, thus n and C_n could be treated as disposable parameters to fit the calculated data, and so could η. Rather than doing this, we have fixed n at its leading value, and determined the other two by a least-squares fitting procedure. Such an approach may be justified by the fact that the range of temperatures is too narrow, thus enhancing a strong correlation between the parameters. All points have been assigned an equal weight of unit in the least-squares fitting procedure, which leads to $C_4 = 18.5$ kcal mol^{-1} Å^n, and $\eta = 1.6$ Å. Clearly, the fit provides a reliable representation of all calculated points, with a root-mean-square deviation of 6.9×10^{-13} cm^3 s^{-1}. Of course, besides the electrostatic interaction between the "relaxed" permanent quadrupole moment of $O(^3P)$ and the permanent dipole moment of OH that varies as r^{-4}, there are further attractive

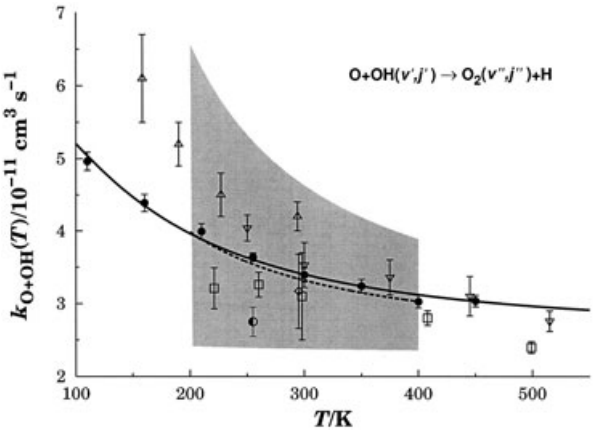

Figure 5. *Thermal rate coefficient as a function of temperature for the reaction $O+OH(v')\rightarrow O_2+H$. The solid circles (●) indicate the QCT results from the present work and corresponding 68% error bars, the half-filled circle the QCT result[80] for v = 0, and the solid line (——) the fit using Equation (34). The other symbols show experimental measurements: ⊡, ref. [84]; ▽, ref. [85]; △, ref. [86]; ◇, ref. [87]. Also shown by the dashed line (-----) are the recommended[81] data, with the uncertainty indicated by the shaded area.*

contributions (of electrostatic, induction, and dispersion types) which have been omitted (see ref. [83] and references therein), and hence the fitted parameters should not be given undue physical meaning. Finally, we show in Figure 5 the best (more recent) available thermally equilibrated measurements[84–87] as well as the recommended[81] value of $k(T) = 2.3\times10^{-11}\exp(110/T)$ cm^{3}s^{M_1} for $200 \le T/K \le 400$. Lewis and Watson's[84] results were obtained from low-pressure flow-discharge resonance fluorescence measurements, with the OH radicals being formed by the reaction of H atoms (produced in a microwave discharge) with NO_2. In turn, Howard and Smith[85] and Smith and Stewart[86] used photolytic methods to produce the OH radicals (photolysis of H_2O by using a flash lamp, and photolysis of HNO_3 at 266 nm by a pulsed laser, respectively). A similar technique was utilized by Robertson and Smith[87] for their experiments at $T = 295$ K, in which the photolysis of ozone was used to measure the O+OH rate constant. Such experiments monitor only changes in concentration of $OH(v'=0)$, and thus the measurements should in no way be affected by differences in the rate constants for the O+OH reactions with distinct vibrational levels of OH. However, there are visible differences amongst the experimental data, with the results of Howard and Smith[85] and Smith and Stewart[86] being generally larger than those of Lewis and Watson[84] and Robertson and Smith.[87] This may in principle be attributed to possible ways of regenerating $OH(v'=0)$. The pulsed photolysis experiments of Howard and Smith[85] and Smith and Stewart[86] are believed[88] to create $OH(v'=0)$ virtually exclusively, so therefore we examine the other two cases. In Lewis and Watson's[84] experiments, a potential problem may be that a slight excess of NO_2 is added to the H atoms, which means that, as H atoms are regenerated by the $O+OH(v'=0)$ reaction, they might react with NO_2 and regenerate OH (although this may be formed in several vibrational levels, some will be produced in $v'=0$ while the remainder is likely to be efficiently relaxed to

$v'=0$ via collisions with NO_2). The situation may be somewhat more problematical in the case of Robertson and Smith's[87] experiments at $T=295$ K, because both the primary formation process and the secondary reaction of H atoms with O_3 are expected to produce high concentrations of OH(v'). Although they too only observe OH($v'=0$), the OH generated in higher vibrational levels could be relaxed into $v'=0$ at a rate comparable to the removal of OH($v'=0$) by reaction. Whether this may explain their somewhat lower measurement for the rate constant (this is nearly coincident with the result of Lewis and Watson[84] for the same temperature, and embraces within the error bars our own QCT result[80] for $v'=0$ at $T=255$ K) remains, of course, an unsettled issue. In summary, the above experiments should undoubtedly be compared with QCT results for O + OH($v'=0$), and hence the agreement of our vibrationally averaged curve with the recommended one may partly be fortuitous. Unfortunately, as far as we are aware, there are no experiments that provide information about the result of collisions between OH($v'>0$) and O atoms. Theoretically, the predicted[80] vibrationally specific rate constant is smaller (larger) for $1\le v'\le 3$ ($4\le v'\le 9$) than for $v'=0$. If thermal equilibrium is not established, as is likely to be the case in the upper atmosphere, one then requires the corresponding vibrationally averaged rate constant. It is therefore striking to observe that the latter closely matches the recommended rate constant for the O + OH($v'=0$) reaction, which turns out to be the one commonly used in atmospheric modeling.

3.2. The O + HO_2 Reaction

Three possible mechanisms can be offered for the title reaction:

$$O_a + HO_bO_c(E_{vib}) \rightarrow O_aH(v'',j'') + O_bO_c(v'',j'') \quad (35)$$

$$O_a + HO_bO_c(E_{vib}) \rightarrow O_bH(v'',j'') + O_aO_c(v'',j'') \quad (36)$$

$$O_a + HO_bO_c(E_{vib}) \rightarrow O_aO_b(v'',j'') + HO_c(v'',j'') \quad (37)$$

where $HO_bO_c(E_{vib})$ stands for a specified initial vibrational energy distribution of the reactant triatomic species, as discussed in Section 2. The barrier for O_a to attack O_b is high, and hence the possibility of reaction (37) occurring should be negligibly small for translational energies of practical relevance when HO_2 is in its ground vibrational state, but the situation may here be distinct since one allows for high vibrational excitations of the hydroperoxyl radical. Similar considerations apply to the attack of O_a on H, although it involves a large activation energy barrier (about 18 kcal mol^{-1}) according to both the DMBE I and DMBE II potential energy surfaces for HO_3. Note that the classical barrier height for isomerization, $HO_bO_c \leftrightarrow O_bO_cH$, is 40.7 kcal mol^{-1}. Thus, for vibrational excitations that allow isomerization, reaction (36) may actually occur via the attack of O_a on the terminal oxygen atom of the O_bO_cH isomer.

Some further remarks concerning the optimization of the impact parameter are in order at this point. One would like to have a value of b_{max} valid for all reactive channels, but we must discard from the analysis at least those leading to O_2 + O + H and OH + O + O. In fact, many of the radicals have an internal vibrational excitation above both the O_2 + H and OH + O asymptotes, and hence reaction may occur even for infinitely large values of b_{max}. The rate constants reported for such reactions may therefore have uncertainties larger than the actually reported error bars. We emphasize that the optimization procedure can be rather time-consuming for the title four-atom reaction, especially for DMBE II, since this is somewhat more complicated than DMBE I and requires numerical derivatives. Thus, we have found the following strategy useful. First, b_{max} is optimized within a few percent for a temperature of $T=300$ K. A first estimate of the maximum impact parameter for other temperatures is then obtained by using $b_{max}^{O+HO_2}(T) = \frac{b_{max}^{O+HO_2}(T=255\,K)}{b_{max}^{O+OH}(T=255\,K)} b_{max}^{O+OH}(T)$, where $b_{max}^{O+OH}(T)$ is the value optimized for the O + OH reaction. Some fine-tuning of the values so obtained is then performed, such that fewer than two trajectories in a total of 5000 (0.04%) fall into the last bin of the opacity functions for reactions (35)–(37). The set of values obtained in this way for DMBE I was then adopted for running the trajectories in DMBE II, since the opacity functions of both potential energy surfaces are expected to be quite similar. In fact, such estimates of b_{max} for DMBE II turned out to be quite reliable, at least for temperatures over the range $210\le T/K\le 300$ that are of special concern here.

We now examine the various collisional outcomes. The salient features from Table 2 and Table 3 are the many channels that become open for reaction and, most importantly, the fact that one of those channels produces two oxygen atoms. Such a reactivity stems from the high initial vibrational excitations considered for HO_2, while the calculated probabilities may be rationalized from the observations made above which are common to both the DMBE I and DMBE II potential energy surfaces: a) the attachment of the colliding oxygen atom to the terminal oxygen atom of HO_2 is easier than to the middle oxygen atom or the H atom end (in this order); b) such differences are attenuated with vibrational excitation of HO_2; for example, the ordering of the reactive probabilities for the channel leading to O_2 + HO may be explained simply by using (a), while the major trends in other channels may be rationalized using (a) and (b) jointly. In turn, one may rationalize the fact of O_bO_c + H + O_a being the dominant outcome simply by recalling that many of the initial HO_bO_c species have an internal energy above the O_bO_c + H asymptote prior to initiating the collisional process. Stable ozone molecules can be directly formed, but most such species have an internal energy above dissociation, and hence they have all been boxed as if the break-off of O_3^* had occurred. Indeed, conversely to DMBE I where O_3^* is produced, DMBE II tends to yield O_3. Classically, this means that the potential energy of O_3 is below that of O_2 + O, even if by a very small amount. It should be emphasized that the two events are hardly distinguishable, while any atomic oxygen that is formed will ultimately recombine with O_2 in the pres-

Table 2. *A summary of some of the dynamics calculations[a] for the $O_a+HO_bO_c$ reaction in the DMBE I potential energy surface.*

			$O+HO_2$[b]		$OH+O_2$[c]		O_2+H+O[d]		$OH+2O$[e]	
T [K]	b_{max} [Å]	$N/10^3$	P_r [%]	$k^{[f]}$ [$cm^3 s^{-1}$]	P_r [%]	$k^{[f]}$ [$cm^3 s^{-1}$]	P_r [%]	$k^{[f]}$ [$cm^3 s^{-1}$]	P_r [%]	$k^{[f]}$ [$cm^3 s^{-1}$]
160	13.0	5	27.1	210.2±4.9	4.4	34.3±2.3	2.1	16.7±1.6	0.0	0.0±0.0
			0.6	5.0±0.9	1.7	12.9±1.4	0.0	0.0±0.0	3.5	27.3±2.0
			0.2	1.6±0.5	0.2	1.4±0.5	59.4	461.5±5.0	0.8	5.9±1.0
			27.9	216.7±4.9	6.3	48.6±6.3	59.5	478.2±5.4	4.3	33.2±2.2
					6.0	46.9±6.0			4.5	35.0±2.3
210	12.3	5	27.2	201.2±4.6	4.7	35.0±2.2	3.8	27.9±2.0	0.0	0.0±0.0
			0.5	3.4±0.7	1.8	13.6±1.4	0.1	0.4±0.3	3.4	25.4±1.9
			0.2	1.5±0.5	0.3	1.9±0.5	57.2	422.7±5.2	0.8	5.9±0.9
			27.9	206.1±4.7	6.8	50.5±2.6	61.1	451.0±5.1	4.2	31.3±2.1
					6.5	47.9±2.6			4.6	34.0±2.2
255	12.0	15	28.6	210.5±2.7	4.0	29.7±1.2	4.0	29.4±1.2	0.0	0.0±0.0
			0.8	5.6±0.5	1.9	14.3±0.8	0.0	0.3±0.1	3.7	27.4±1.1
			0.3	2.2±0.3	0.2	1.5±0.3	55.7	410.5±3.0	0.8	6.0±0.5
			29.7	218.3±2.8	6.1	45.5±1.4	59.7	440.2±3.0	4.5	33.4±1.2
					5.7	42.3±3.0			4.9	36.4±1.3
300	11.5	5	27.2	192.0±4.4	4.5	29.5±2.0	4.7	33.2±2.1	0.0	0.0±0.0
			0.7	5.0±0.8	2.1	14.6±1.4	0.0	0.1±0.1	3.5	24.7±1.8
			0.1	1.0±0.4	0.3	1.8±0.5	56.5	399.5±5.0	0.7	5.1±0.8
			28.0	198.0±4.5	6.5	45.9±2.5	56.6	432.9±4.9	4.2	29.8±2.0
					6.1	43.1±2.4			4.6	32.5±2.1

[a] The optimum step size for numerical integration was 8×10^{-15} s, with the trajectories initiated for the reactants 13 Å apart from each other at $T=110$ K (not tabulated), where this separation was 14 Å. [b] The first entry refers to $O_a+HO_bO_c$, the second to $O_c+HO_bO_a$, and the third to $O_b+HO_cO_a$. [c] The first entry refers to $O_aO_c+O_bH$, the second to $O_aO_b+O_cH$, and the third to $O_bO_c+O_aH$. [d] The first entry refers to $O_cO_a+H+O_b$ or $H+O_3^*$, the second to $O_aO_b+H+O_c$, and the third to $O_bO_c+H+O_a$. [e] The first entry refers to $O_aH+O_b+O_c$, the second to $O_bH+O_a+O_c$, and the third to $O_cH+O_a+O_b$. [f] All rate constants should be multiplied by 10^{-12}. In all cases, the fourth entry represents the sum of the other three. Where appropriate, the fifth entry gives the total rate constant after correcting for dissociative and predissociative diatomics.

Table 3. *A summary of the dynamics calculations[a] for the $O_a+HO_bO_c$ reaction in the DMBE II potential energy surface.*

			$O+HO_2$[b]		$OH+O_2$[c]		O_2+H+O[d]		$OH+2O$[e]	
T [K]	b_{max} [Å]	$N/10^3$	P_r [%]	$k^{[f]}$ [$cm^3 s^{-1}$]	P_r [%]	$k^{[f]}$ [$cm^3 s^{-1}$]	P_r [%]	$k^{[f]}$ [$cm^3 s^{-1}$]	P_r [%]	$k^{[f]}$ [$cm^3 s^{-1}$]
210	12.2	5	30.0	218.2±4.7	3.7	27.2±2.0	3.7	26.8±1.9	0.0	0.1±0.1
			0.7	4.8±0.8	1.6	11.8±1.3	0.1	0.9±0.4	4.1	29.5±2.0
			0.1	0.9±0.4	0.2	1.5±0.5	55.0	399.8±5.1	0.8	5.8±0.9
			30.8	223.9±4.7	5.5	40.5±2.4	58.8	427.5±5.1	4.9	35.4±2.2
					5.3	38.8±2.3			5.1	37.1±2.3
255	12.0	5	30.2	222.8±4.8	3.4	24.9±1.9	4.2	31.1±2.1	0.0	0.0±0.0
			0.4	3.2±0.7	1.8	13.6±1.4	0.0	0.2±0.2	3.7	27.3±2.0
			0.1	0.9±0.4	0.2	1.6±0.5	54.9	405.1±5.2	0.9	6.6±1.0
			30.7	226.9±4.8	5.4	40.1±2.4	59.1	436.4±5.2	4.6	33.9±2.2
					5.1	37.6±2.3			4.9	36.0±2.2
300	11.5	5	30.4	214.8±4.6	3.4	24.2±1.8	4.8	34.3±2.1	0.0	0.0±0.0
			0.5	3.2±0.7	1.6	11.2±1.2	0.0	0.3±0.2	3.6	25.6±1.9
			0.1	1.0±0.4	0.3	1.8±0.5	54.2	382.8±5.0	1.0	7.3±1.0
			31.0	219.0±4.6	5.3	37.2±2.2	59.0	417.4±5.0	4.6	32.9±2.1
					5.0	35.0±2.2			4.9	34.9±2.2

[a] The optimum step size for numerical integration was 8×10^{-15} s, with the trajectories initiated for the reactants 13 Å apart from each other except at $T=110$ K where this separation was 14 Å. [b] The first entry refers to $O_a+HO_bO_c$, the second to $O_c+HO_bO_a$, and the third to $O_b+HO_cO_a$. [c] The first entry refers to $O_aO_c+O_bH$, the second to $O_aO_b+O_cH$, and the third to $O_bO_c+O_aH$. [d] The first entry refers to $O_cO_a+H+O_b$ or $H+O_3^*$, the second to $O_aO_b+H+O_c$, and the third to $O_bO_c+H+O_a$. [e] The first entry refers to $O_aH+O_b+O_c$, the second to $O_bH+O_a+O_c$, and the third to $O_cH+O_a+O_b$. [f] All rate constants should be multiplied by 10^{-12}. In all cases, the fourth entry represents the sum of the other three. Where appropriate, the fifth entry gives the total rate constant after correcting for dissociative and predissociative diatomics.

ence of a third body to produce O_3. Similar considerations apply to the channels (35)–(37). In fact, we have considered as forming $OH+O_2$ only the trajectories where both products finished with an internal energy below dissociation. Thus, we have excluded trajectories leading to species with an energy above the centrifugal barrier as well as metastable ones that could predissociate (i.e., with an internal energy above the dissociation threshold). For $T=255$ K, this leads to a decrease by about 6% of the rate constant for $OH+O_2$ formation, while enhancing by the same amount the rate constant for production of two oxygen atoms. Note that the channel forming O_2+H+O is neutral in the sense of null odd-oxygen (ozone) de-

struction, whereas the channel yielding OH+O+O is a novel ozone source: for each destroyed oxygen atom two new ones are formed. Both such channels should be particularly active in the mesosphere where vibrationally hot OH radicals are abundant[6,75] (they may then form highly vibrationally excited HO_2 when reacting with ozone).

We now turn to the vibrational energy distributions of the product molecules originating from both nonreactive and reactive $O+HO_2$ collisions: for example, for $T=210$ K, they represent 29% (23%) of the total number of trajectories run in the DMBE I (DMBE II) potential energy surface. Essentially, all molecules end up with a vibrational energy above the ZPE. Of course, classically, if an HO_2 species is produced having an internal energy above the $H+O_2$ dissociation energy of ≈ 57.1 kcal mol^{-1}, it will lead to $H+O_2$ unless a collision occurs that may alter the course of the dissociation process. Moreover, if such an HO_2^* species has an energy exceeding ≈ 68.3 kcal mol^{-1}, it may instead lead to O+O+OH. In fact, 68.62% (35.4%) of the HO_2 molecules in the nascent distribution have a vibrational energy over the classical $H+O_2$ (O+OH) dissociation limit, a result that overpasses significantly the sum of the fractions of reactive trajectories leading to H+O+O_2 and O+O+OH, respectively 49.2 and 4.5% at 210 K. The remaining trajectories (31.4%) are therefore either nonreactive, in the sense of leading to HO_2/HO_2^*, or have a different outcome. If we then sum the trajectories yielding $H+O+O_2$ and O+O+OH with those forming $O+HO_2/HO_2^*$ (28%), we obtain the total number of trajectories that produce HO_2/HO_2^*. They represent 82.3% of the total at 210 K, a value that shows a striking similarity to the fraction of OH (86.3%) formed in the O+OH reaction at the same temperature (a similar trend is observed for other temperatures). Figure 6 compares, for $T=$ 255 K, the vibrational distribution of such HO_2/HO_2^* species

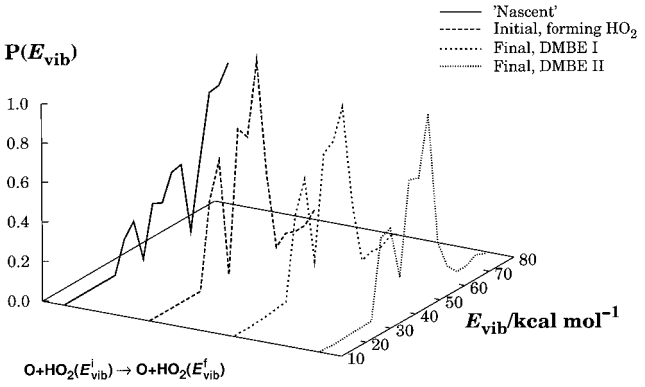

Figure 6. Final vibrational energy distributions of hydroperoxyl radicals in $O+HO_2$ nonreactive encounters using DMBE I and DMBE II potential energy surfaces.

with the initial (forming HO_2/HO_2^*) and "nascent" distributions. As in the case of O+OH, the striking feature is the remarkable similarity of the final and initial vibrational distributions of HO_2/HO_2^*, which reinforces our belief that such vibrationally hot species may also be relatively abundant at high altitudes. Of course, a more realistic assessment requires consideration of the vibrational relaxation of HO_2/HO_2^* in collisions with major atmospheric constituents, such as N_2 and O_2.

In Figure 7 we show a 2D plot of the vibrational–rotational distribution of the OH(v'',j'') formed via reaction (35), while the rotational distribution corresponding to the maximum of the OH vibrational distribution is in Figure 8. Clearly, the large var-

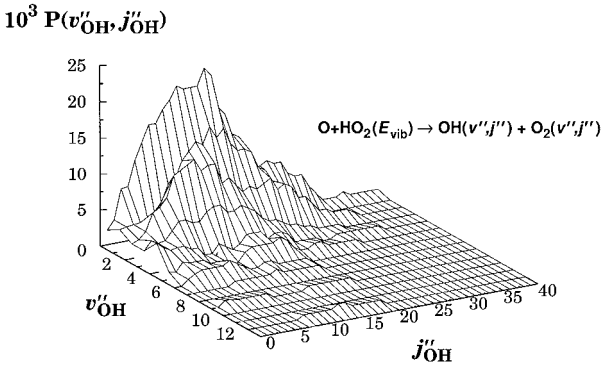

Figure 7. Rovibrational distribution of product OH(v'',j'') from the LTD $O+HO_2$-(E_{vib}) reactive collisions at a temperature of 255 K.

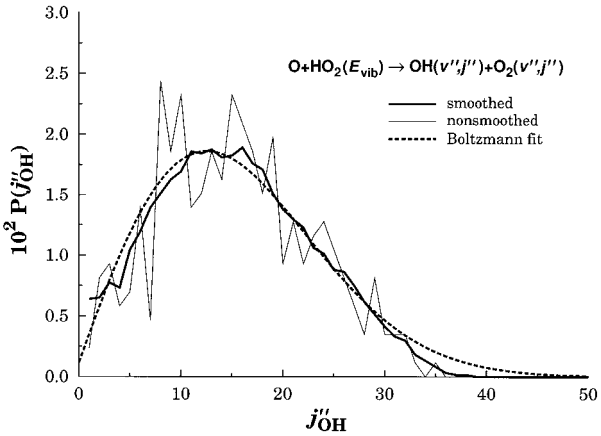

Figure 8. Rotational distribution of product OH(v'',j'') from the LTD $O+HO_2$(E_{vib}) reactive collisions corresponding to the maximum value of v'' at $T=255$ K.

iations in the relative population of adjacent rotational levels are partly a result of incomplete convergence of the distribution. To smooth out such a distribution, we averaged neighboring rotational states by using standard smoothing techniques.[89] Specifically, we used a moving-window averaging procedure (see also refs. [90,91]), which consists of replacing each data value by an average of itself and six near neighbors, three to the left and three to the right. The smoothed curve is shown by the thick solid line. It is seen that the product OH vibrational distribution shows a maximum for $v''=0$, with the population declining fast to become rather small at $v''=6$. Yet, vestige occupations are seen even for OH vibrational levels as high as $v''=14$. It is hard to say whether the rotational distribution is of the Boltzmann type, but we show by the least-squares fit (dashed line) that it corresponds roughly to a tem-

perature of 9244 K. Such a rotational warming may be attributed to the fact that the exothermicity of the reaction (including the internal excitation of the reactants) is channeled into HO_2 and randomized before the O–O bond breaks off to form another O–O bond with the incoming oxygen atom. It also suggests that the OH bond acts as a spectator in the sense that it remains thermalized even after the products are formed. Finally, we observe from Figure 8 that rotational states as high as $j''=35$ are populated for low vibrational states. This is an interesting result since there is strong evidence from the mesosphere that rotational levels as high as 30–33 are present[92] (see also ref. [39]).

Unfortunately, it is unaffordable to run a sufficient number of trajectories to show a 2D vibrational–rotational plot for the $O_2(v'',j'')$ products due to the large number of occupied states. Thus, similarly to O+OH, we show in Figure 9 the vibrational

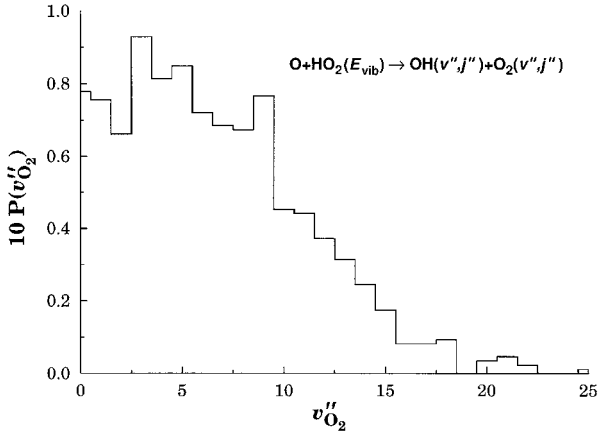

Figure 9. *Vibrational distribution of product $O_2(v'',j'')$ from the LTD $O+HO_2(E_{vib})$ reactive collisions at a temperature of 255 K.*

distribution of O_2 obtained for all vibrational energies of the reactants HO_2 sampled at $T=255$ K. It is a slightly inverted population that peaks at about $v''=3$ before decaying slowly to assume negligible values at $v''>25$. As regards the corresponding rotational distribution, we simply note that it shows characteristics rather similar to those of the O_2 produced in the O+OH reaction at the same temperature, except for the fact that even higher rotational states are populated. In fact, it is well described by a Boltzmann distribution with a characteristic rotational temperature of $T=30\,413$ K. This is about twice as large as that obtained in the O+OH case, which may be explained from the fact that the classical exothermicity is significantly larger (13.41 kcal mol^{-1} vs. 51.94 kcal mol^{-1}) in the case of the reaction $O+HO_2\rightarrow OH+O_2$.

Finally, we address the effect of vibrationally exciting HO_2 in the thermal rate constant for the reaction $O+HO_2\rightarrow O_2+OH$. Figure 10 shows the rate constants calculated from both the DMBE I and DMBE II potential energy surfaces, as well as the fit to the DMBE I results based on Equation (34). Since $k(T)$ for DMBE II was calculated only at three temperatures, no attempt was made to fit the corresponding results. Note that the elec-

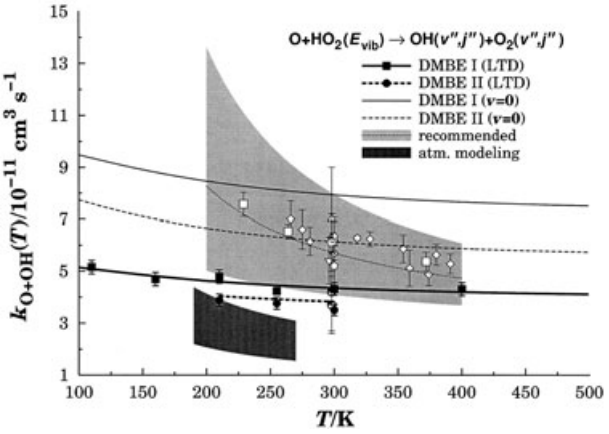

Figure 10. *Influence of vibrational excitation in the rate constant for the reaction $O+HO_2(E_{vib})\rightarrow O_2+OH$ and comparison with experimental data,[94–102] which are shown by the open symbols. The thin lines indicate the results obtained in DMBE I and DMBE II when E_{vib} is fixed at the ZPE. The results obtained with DMBE I when the vibrational energy distribution of HO_2 is the nascent one from the reaction $OH(v)+O_3\rightarrow HO_2+O_2$ is shown by the corresponding thick solid line and squares (■). The solid circles (●) with error bars indicate the results for DMBE II, while the thick dashed line represents a downscaling of the DMBE I fit by 12%. The shaded areas show the uncertainties in the recommended[81] rate constant (light gray) and its downrevision[26] to improve the correspondence between the O_3 production and destruction rates (gray).*

tronic degeneracy factor is now $f_e(T)=1/[5+3\exp(-228/T)+\exp(-326/T)]$. There is only a small variation of $k_7(T)$ with the temperature, but for consistency we use the capture plus hard-spheres model in Equation (34). Except for the point at $T=255$ K that was given a weight of three, all others carried a weight of unity in the least-squares fitting procedure. With n fixed at $n=4$, this leads in the case of DMBE I to $C_n=20.4302$ kcal mol^{-1} and 1.3316 Å, with associated errors of 17 and 29%, respectively. As for the O+OH reaction, the strong correlation between the parameters suggests that their physical significance should be seen with caution. Also shown for comparison in Figure 10 are the results calculated for a vibrational energy of HO_2 equal to the ZPE,[93] as well as the available experimental measurements[94–102] and the recommended[81] value of $k_7(T)=2.7\times10^{-11}\exp(224/T)$ cm^3 s^{-1} which is valid over the temperature range $200\leq T/K\leq400$. The significant result is that $k_7(T)$ is inhibited by vibrationally exciting HO_2 when compared with the case[93] where HO_2 is initially in the ground vibrational state, although its magnitude still fits within the error bars of the recommended[81] rate constant (except, perhaps, at low temperatures). For example, at $T=255$ K, such a decrease is 44% for DMBE I and 36% for DMBE II. This may be rationalized from the fact that, for a fixed vibrational excitation[93] of HO_2, the rate constant increases slightly more in the case of DMBE II than in the case of DMBE I. However, such a discrepancy diminishes when considering the LTD micropopulation for HO_2, since there is a high fraction of HO_2^* species that reacts via other channels. To see this, we show in Figure 10 a line obtained by downscaling 12% the fit to the DMBE I results, to match the value calculated for $T=255$ K using DMBE II. Clearly, the required downscaling is smaller than the value of 22% predicted from the calculated rate constants when HO_2 has ZPE.

4. Possible Implications in Atmospheric Modeling

To discuss possible implications in atmospheric modeling, we begin with the above observation that the values of k_7 calculated using the micropopulations considered in the present work are roughly 45% (35%) smaller for DMBE I (DMBE II) than those obtained with HO_2 at ZPE. Such a difference tends, for DMBE I, to increase slightly with decreasing temperature over the range of interest, $170 \leq T/K \leq 270$, with a similar trend being possibly applicable to DMBE II. This finding implies that the value $k_7(T)$ used in modeling studies of the middle atmosphere should be downscaled by the same amount. Interestingly, such a prediction agrees qualitatively with the suggestion of Summers et al.,[26] who proposed downward revisions of the recommended[81] rate constant k_7 (supposedly for the thermalized reactants) by as much as 50–75% to improve the correspondence between the ozone production and destruction rates. Thus, the fact that their value significantly exceeds the uncertainty in the recommended value of k_7 may not necessarily imply difficulties in the measurements,[81,94–102] but simply that their proposed rate constant should mimic conditions of LTD. We recall that their downrevision underestimates[24] the observed abundances of OH and HO_2.

Another parameter that has been the subject of optimization in atmospheric modeling is the ratio k_7/k_6. Figure 11 compares the result predicted from our calculations with that ("recommended ratio") obtained from the recommended[81] rate constants where the reactants are assumed to be thermalized. Our calculated rate constants, obtained by using DMBE I for the $O + HO_2$ reaction, are seen to predict a value of k_7/k_6 that supports a downrevision of the "recommended ratio" by 25–30% over the range $170 \leq T/K \leq 270$. Such a revision widens slightly (25–40%) when one includes the results from DMBE II. Thus, the values show a striking agreement with the suggestion of Sandor and Clancy,[27] who propose a downrevision of the "recommended ratio" by 25% (as well as either a 25% reduction in the rate constant of the reaction $OH + HO_2 \rightarrow O_2 + H_2O$ or a 25% increase in HO_x production) when reproducing the measured concentrations of OH and HO_2 above 38 km. Our proposed reduction is also fully consistent with the uncertainties in the recommended rate constants, although it is the result of assuming LTD at such altitudes. To the extent that our potential energy surfaces are realistic, the above agreement between the calculated scaling factors and those obtained from atmospheric modeling emerges as supporting evidence of LTD in the middle atmosphere.

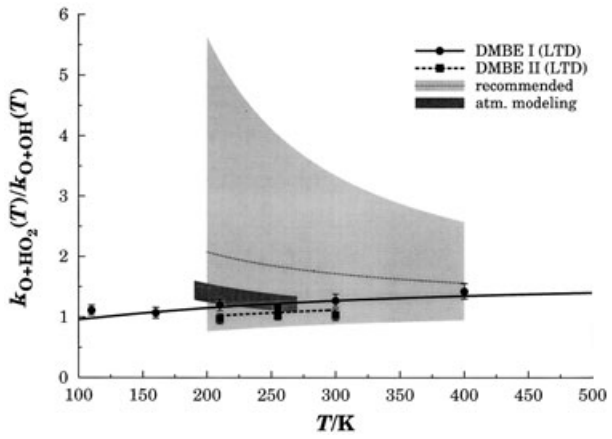

Figure 11. *A comparison of the ratio k_7/k_6 predicted from the calculated rate constants (symbols as in Figure 10) for the title reactions with that (-----) obtained from their recommended[81] values. The shaded areas show the uncertainties due to those in the recommended[81] rate constant (light gray), and its downrevision by 25–40% (gray) which includes, as the lower bound, the one suggested by Sandor and Clancy[27] to reproduce the measured [OH] and [HO_2] above 38 km.*

Despite the fact that downscaling the rate constant of reaction (7) or the ratio of reactions (7) and (6) finds support in the LTD dynamics studies presented here, it is well established[28] that such downrevisions of the standard kinetics parameters are unable by themselves to resolve the long-standing "ozone deficit problem" above 45 km or the HO_x dilemma in the middle atmosphere. A most interesting feature from the present calculations is therefore the fact that they also alert for the production of atomic hydrogen and odd-oxygen species (via the reactions $O + HO_2 \rightarrow O_2 + H + O$ and $O + HO_2 \rightarrow OH + O + O$) that may play a significant role in the HO_2/OH partition and ozone formation at such altitudes. Note that, although atomic hydrogen is traditionally viewed to form HO_2 in the presence of a third body, it may have a more subtle participation in the HO_2/OH partition as suggested in ref. [6]. Thus, our recently proposed theory,[6] jointly with some downrevision of either k_7 or k_7/k_6, may help to unravel mysteries that have been pending for two decades in the chemistry of the middle atmosphere. These findings also set in perspective the basic features for future LTD atmospheric modeling.

5. Concluding Remarks

In previous papers,[5,6,39] we have shown that vibrationally excited species, such as O_2, OH, and HO_2, may offer clues to ozone-related problems in the middle atmosphere. Of special relevance was the observation that the "ozone deficit problem" and "HO_x dilemma" were interrelated, and that both could be rationalized from the mechanisms (9)–(17) and (18)–(27). However, the important question whether such a vibrational excitation would affect the title ozone sink reactions, and hence disturb the impact of the suggested mechanisms, was left unanswered in those papers. The results from the present work have not only provided evidence that corroborates our theory,[6] but also explained why some downscaling of k_7 or the ratio k_7/k_6 may additionally be justified to bring theory and observation into agreement. In so doing, they also offer strong evidence that LTD cannot be ignored in modeling the middle atmosphere. Naturally, one should be aware of the difficulties in obtaining accurate (often multisheeted[103]) potential energy surfaces for the title systems, as well as of the fact that nonadiabatic effects have here been ignored. Previous results[18,42,73] suggest that quantum effects may have no dramatic implica-

tions for the title reactions, but the present work may also provide additional motivation for carrying out studies that include such effects. Similarly, although the use of "nascent" rather than a "steady-state" vibrational distribution for HO_2 may not invalidate the major trends here reported for the $O+HO_2$ reaction, only vibrational relaxation studies of this triatomic molecule may help in deciding such an issue. In summary, both analytical and modeling studies that merge together the information gathered in this and previous work[5,6,39] would be valuable. The use of the new results to extract altitude profiles for specific OH vibrational states is hopefully also envisaged.

Acknowledgements

The author wishes to thank Professor I. W. Smith (U.K.) for helpful correspondence. This work has the financial support of Fundação para a Ciência e a Tecnologia, Portugal, via programs POCTI/40154/QUI/2001 and FEDER.

Keywords: atmospheric chemistry · kinetics · ozone · radical reactions · thermodynamics

[1] T. E. Graedel, P. J. Crutzen, *Atmospheric Change*, Freeman, New York, **1993**.
[2] T. G. Slanger, *Science* **1994**, *265*, 1817.
[3] H. Parker, T. G. Slanger, *J. Chem. Phys.* **1994**, *100*, 287.
[4] C. A. Rogaski, J. M. Price, J. A. Mack, A. M. Wodtke, *Geophys. Res. Lett.* **1993**, *20*, 2885.
[5] A. J. C. Varandas, *ChemPhysChem* **2002**, *3*, 433.
[6] A. J. C. Varandas, *J. Phys. Chem. A* **2004**, *108*, 758.
[7] C. A. Rogaski, J. A. Mack, A. M. Wodtke, *Faraday Discuss.* **1995**, *100*, 229.
[8] J. M. Price, J. A. Mack, C. A. Rogaski, A. M. Wodtke, *Chem. Phys.* **1993**, *175*, 83.
[9] R. Hernández-Lammoneda, R. Toumi, D. C. Clary, *J. Chem. Phys.* **1995**, *102*, 9544.
[10] N. Balakrishnan, G. D. Billing, *Chem. Phys. Lett.* **1995**, *242*, 68.
[11] A. J. C. Varandas, W. Wang, *Chem. Phys.* **1997**, *215*, 167.
[12] R. Hernández-Lamoneda, M. I. Hernández, E. Carmona-Novillo, J. Campos-Martínez, J. Echave, D. C. Clary, *Chem. Phys. Lett.* **1997**, *276*, 152.
[13] W. Wang, A. J. C. Varandas, *Chem. Phys.* **1998**, *236*, 181.
[14] J. Campos-Martínez, E. Carmona-Novillo, J. Echave, M. I. Hernández, R. Hernández-Lamoneda, J. Palma, *Chem. Phys. Lett.* **1998**, *289*, 150.
[15] D. Lauvergnat, D. Clary, *J. Chem. Phys.* **1998**, *108*, 3566.
[16] N. Balakrishnan, A. Dalgarno, G. D. Billing, *Chem. Phys. Lett.* **1998**, *288*, 657.
[17] R. Hernández-Lamoneda, A. Ramírez-Solis, *J. Chem. Phys.* **2000**, *113*, 4139.
[18] A. J. C. Varandas, *Int. Rev. Phys. Chem.* **2000**, *19*, 199.
[19] R. T. Jongma, S. Shi, A. M. Wodtke, *J. Chem. Phys.* **1999**, *111*, 2588.
[20] R. T. Clancy, D. W. Rusch, R. J. Thomas, M. Allen, R. S. Eckman, *J. Geophys. Res.* **1987**, *92*, 3067.
[21] M. A. J. Eluszkiewicz, M. Allen, *J. Geophys. Res.* **1993**, *98*, 1069.
[22] R. L. Miller, A. G. Suits, P. L. Houston, R. Toumi, J. A. Mack, A. M. Wodtke, *Science* **1994**, *265*, 1831.
[23] P. J. Crutzen, J. U. Grooß, C. Brühl, R. Müller, J. M. Russell III, *Science* **1995**, *268*, 705.
[24] G. B. Osterman, R. J. Salawitch, B. Sen, G. C. Toon, R. A. Stachnik, H. M. Pickett, J. J. Margitan, J. Blavier, D. B. Peterson, *Geophys. Res. Lett.* **1997**, *24*, 1107.
[25] R. R. Conway, M. E. Summers, M. H. Stevens, J. G. Cardon, P. Preusse, D. Offermann, *Geophys. Res. Lett.* **2000**, *27*, 2613.
[26] M. E. Summers, R. R. Conway, D. E. Siskind, M. H. Stevens, D. Offermann, M. Riese, P. Preusse, D. F. Strobel, J. M. Russell III, *Science* **1997**, *277*, 1967.
[27] B. J. Sandor, R. T. Clancy, *J. Geophys. Res.* **1998**, *103*, 13 337.
[28] K. W. Jucks, D. G. Johnson, K. V. Chance, W. A. Traub, J. J. Margitan, G. B. Osterman, R. J. Salavitch, Y. Sasano, *Geophys. Res. Lett.* **1998**, *25*, 3935.
[29] A. J. C. Varandas, A. A. C. C. Pais, J. M. C. Marques, W. Wang, *Chem. Phys. Lett.* **1996**, *249*, 264.
[30] J. M. C. Marques, W. Wang, A. A. C. C. Pais, A. J. C. Varandas, *J. Phys. Chem.* **1996**, *100*, 17 513.
[31] One may infer from previous dynamics studies[29,30] on the reaction $H+ArO_2 \rightarrow Ar+HO_2$ that HO_2 is possibly formed in a highly vibrationally excited state, but it would be interesting to perform similar studies with the active species O_2 acting itself also as the chaperon, which could be done by employing our recently reported double many-body expansion (DMBE) potential energy surface[32] for the electronic ground state of HO_4.
[32] A. J. C. Varandas, L. Zhang, *Chem. Phys. Lett.* **2000**, *331*, 474.
[33] k_n denotes the rate constant for reaction (*n*).
[34] Note that the middle of Equation (41) of ref. [6] has a misprint: the symbol $\approx$ preceding $[O_3]/[M]$ should obviously be eliminated.
[35] P. J. S. B. Caridade, M. Betancourt, J. D. Garrido, A. J. C. Varandas, *J. Phys. Chem. A* **2001**, *105*, 7435.
[36] A. J. C. Varandas, P. J. S. B. Caridade, *Chem. Phys. Lett.* **2001**, *339*, 1.
[37] J. D. Garrido, P. J. S. B. Caridade, A. J. C. Varandas, *J. Phys. Chem. A* **2002**, *106*, 5314.
[38] P. J. S. B. Caridade, J. Sabin, J. D. Garrido, A. J. C. Varandas, *Phys. Chem. Chem. Phys.* **2002**, *4*, 4959.
[39] A. J. C. Varandas, *J. Phys. Chem. A* **2003**, *107*, 3769.
[40] H. Teitelbaum, *Chem. Phys.* **1988**, *124*, 55.
[41] H. Szichman, M. Baer, A. J. C. Varandas, *J. Phys. Chem.* **1998**, *102*, 8909.
[42] A. J. C. Varandas, H. Szichman, *Chem. Phys. Lett.* **1998**, *295*, 113.
[43] W. L. Hase, MERCURY: a general Monte Carlo classical trajectory computer program, QCPE#453. An updated version of this code is VENUS96: W. L. Hase, R. J. Duchovic, X. Hu, A. Komornik, K. F. Lim, D.-H. Lu, G. H. Peslherbe, K. N. Swamy, S. R. van de Linde, A. J. C. Varandas, H. Wang, R. J. Wolf, *QCPE Bull* **1996**, *16*, 43.
[44] M. R. Pastrana, L. A. M. Quintales, J. Brandão, A. J. C. Varandas, *J. Phys. Chem.* **1990**, *94*, 8073.
[45] A. J. C. Varandas, H. G. Yu, *Mol. Phys.* **1997**, *91*, 301.
[46] H. G. Yu, A. J. C. Varandas, *Chem. Phys. Lett.* **2001**, *334*, 173.
[47] A. J. C. Varandas, J. Brandão, M. R. Pastrana, *J. Chem. Phys.* **1992**, *96*, 5137.
[48] Note that only odd rotational states are allowed if OH is considered to belong to Hund's case (b).[106]
[49] Strictly speaking this implies nonvariation with time, a prerequisite that cannot obviously be warranted in our definition.
[50] H. Ohoyama, T. Kasai, Y. Yoshimura, H. Kuwata, *Chem. Phys. Lett.* **1985**, *118*, 263.
[51] P. C. Cosby, private communication, July **2002**.
[52] This effective rotational distribution has in turn been obtained by weighting the rotational distributions actually reported by Cosby[51] for the six OH Meinel bands (4–0, 5–1, 6–1, 7–2, 8–3, 9–4) with the appropriate weights given by the nascent vibrational distribution of Ohoyama et al.[50] Note that the Cosby distributions represent season-averaged values for OH in the nightglow (i.e., created by the $H+O_3$ reaction) subject to some collisional relaxation before emitting. This is most likely responsible[51] for the two-temperature rotational distributions observed in the nightglow data: a low temperature ($\approx$200 K) in the rapidly relaxed lower rotational levels ($j' < 5$) and a much higher apparent temperature in the slowly relaxed higher rotational levels; see Figure 4a of ref. [39]. See also ref. [6].
[53] R. P. Wayne, *Chemistry of Atmospheres, 3rd Ed.*, Oxford University Press, Oxford, **2002**.
[54] L. Zhang, A. J. C. Varandas, *Phys. Chem. Chem. Phys.* **2001**, *3*, 1439.
[55] A. J. C. Varandas, L. Zhang, *Chem. Phys. Lett.* **2001**, *340*, 62.
[56] Note that the threshold translational energy[32] for the $OH(v'=0)+O_3$ reaction is $E_{th}=1.056$ kcal mol^{-1}, which implies that it cannot occur for collisional energies smaller than E_{th}. Of course, this does not mean that reaction cannot occur at an equivalent translational temperature

of 354.3 K. The vibrational population of OH predicted from the steady-state distribution is very small for $v'=0$, therefore such an issue may here be safely ignored.
[57] This is an approximate sampling method due to the significant anharmonicity of the HO_2 and O_3 potential energy surfaces.
[58] A. J. Dobbyn, M. Stumpf, H.-M. Keller, W. L. Hase, R. Shinke, *J. Chem. Phys.* **1995**, *103*, 9947.
[59] J. M. C. Marques, A. J. C. Varandas, *J. Phys. Chem.* **1997**, *101*, 5168.
[60] A. J. C. Varandas, *Chem. Phys. Lett.* **1994**, *225*, 18.
[61] A. J. C. Varandas, J. M. C. Marques, *J. Chem. Phys.* **1994**, *100*, 1908.
[62] S. Kumar, N. Sathyamurthy, R. Ramaswamy, *J. Chem. Phys.* **1995**, *103*, 6021.
[63] M. Ben-Nun, R. D. Levine, *J. Chem. Phys.* **1996**, *105*, 8136.
[64] Y. Guo, D. L. Thompson, T. D. Sewell, *J. Chem. Phys.* **1996**, *104*, 576.
[65] K. F. Lim, *J. Chem. Soc. Faraday Trans.* **1997**, *93*, 669.
[66] A. J. Marks, *J. Chem. Phys.* **1998**, *108*, 1438.
[67] J. A. Miller, *J. Chem. Phys.* **1986**, *84*, 6170.
[68] L. A. M. Quintales, A. J. C. Varandas, J. M. Alvariño, *J. Phys. Chem.* **1988**, *92*, 4552.
[69] J. Davidsson, G. Nyman, *Chem. Phys.* **1988**, *125*, 171.
[70] G. Nyman, J. Davidsson, *J. Chem. Phys.* **1990**, *92*, 2415.
[71] A. J. C. Varandas, J. M. C. Marques, *J. Chem. Phys.* **1992**, *97*, 4050.
[72] G. Nyman, *Chem. Phys.* **1993**, *173*, 159.
[73] J. M. C. Marques, W. Wang, A. J. C. Varandas, *J. Chem. Soc. Faraday Trans.* **1994**, *90*, 2189.
[74] D. C. Clary, H.-J. Werner, *Chem. Phys. Lett.* **1984**, *112*, 346.
[75] S. Adler-Golden, *J. Geophys. Res.* **1997**, *102*, 19969.
[76] Recall that the classical barrier height for O-attacking the H end of OH is about 13.4 kcal mol^{-1}.
[77] The numbers are quoted with a fixed number of digits along the paper; however, this was done only for convenience and by no means invalidates the accuracy expressed by the error bars when given.
[78] We denote by (v'',j'') the vibrational–rotational state of the OH radicals, either formed reactively or nonreactively.
[79] D. E. Osterbrock, J. P. Fulbright, P. Cosby, T. A. Barlow, *Publ. Astron. Soc. Pac.* **1998**, *110*, 1499.
[80] A. J. C. Varandas, *Chem. Phys. Lett.* **2004**, *396*, 182.
[81] R. Atkinson, D. L. Baulch, R. A. Cox, R. F. Hampson, Jr., J. A. Kerr, J. Troe, *J. Phys. Chem. Ref. Data* **1992**, *21*, 1125.
[82] A. J. C. Varandas, *Faraday Discuss. Chem. Soc.* **1987**, *84*, 353.
[83] J. M. C. Marques, A. J. C. Varandas, *Phys. Chem. Chem. Phys.* **2001**, *3*, 2632.
[84] R. S. Lewis, R. T. Watson, *J. Phys. Chem.* **1980**, *84*, 3495.
[85] M. J. Howard, I. W. Smith, *J. Chem. Soc. Faraday Trans. 2* **1981**, *77*, 997.
[86] W. I. Smith, W. A. Stewart, *J. Chem. Soc. Faraday Trans.* **1994**, *90*, 3221.
[87] R. Robertson, G. P. Smith, *Chem. Phys. Lett.* **2002**, *358*, 157.
[88] W. I. Smith, private communication, November **2004**.
[89] W. H. Press, S. A. Teukolsky, W. T. Vetterling, B. P. Flannery, *Numerical Recipes in Fortran: the Art of Scientific Computing*, Cambridge University Press, New York, **1992**.
[90] A. J. C. Varandas, *Mol. Phys.* **1995**, *85*, 1159.
[91] P. J. S. B. Caridade, J. L. Llanio-Trujillo, A. J. C. Varandas, *J. Phys. Chem. A* **2004**, *108*, 10926.
[92] J. A. Dodd, S. J. Lipson, J. R. Lowell, P. S. Armstrong, W. A. M. Blumberg, R. M. Nadile, S. M. Adler-Golden, W. J. Marinelli, K. W. Holtzclaw, B. D. Green, *J. Geophys. Res.* **1994**, *99*, 3559.
[93] D. M. Silveira, P. J. S. B. Caridade, A. J. C. Varandas, *J. Phys. Chem. A* **2004**, *108*, 8721.
[94] J. Peeters, G. Mahnen, *Proc. Combust. Inst.* **1973**, *14*, 133.
[95] M. J. Day, K. Thompson, G. Dixon-Lewis, *Proc. Combust. Inst.* **1973**, *14*, 47.
[96] W. Hack, A. W. Preuss, F. Temps, H. Wagner, *Ber. Bunsenges. Phys. Chem.* **1979**, *83*, 1275.
[97] R. R. Lii, J. M. C. Sauer, S. Gordon, *J. Phys. Chem.* **1980**, *84*, 817.
[98] J. M. Nicovich, P. H. Wine, *J. Phys. Chem.* **1987**, *91*, 5118.
[99] L. F. Keyser, *J. Phys. Chem.* **1982**, *86*, 3439.
[100] U. C. Sridharan, L. X. Qiu, F. Kaufman, *J. Phys. Chem.* **1982**, *86*, 4469.
[101] A. R. Ravishankara, P. H. Wine, B. M. Nicovich, *J. Chem. Phys.* **1983**, *78*, 6629.
[102] W. H. Brune, J. J. Schwab, J. G. Anderson, *J. Phys. Chem.* **1983**, *87*, 4503.
[103] A. J. C. Varandas in *Conical Intersections: Electronic Structure, Dynamics and Spectroscopy, Advanced Series in Physical Chemistry* (Eds.: D. Yarkony, H. Köppel, W. Domcke), World Scientific, Singapore, **2004**, Ch. 5.
[104] G. Herzberg, *Molecular Spectra and Molecular Structure. I. Spectra of Diatomic Molecules, 2nd Ed.*, Van Nostrand, New York, **1950**.
[105] J. R. Le Roy, *Level 7.5: A Computer Program for Solving the Radial Schrödinger Equation for Bound and Quasibound Levels*, Tech. Rep. CP-655, University of Waterloo, Chemical Physics Research Report **2002**.
[106] A. J. C. Varandas, *J. Chem. Phys.* **1993**, *99*, 1076.

Received: July 19, 2004
Revised: November 22, 2004

